

Trigonometric Parallaxes of Massive Star Forming Regions: V. G23.01–0.41 and G23.44–0.18

A. Brunthaler¹, M. J. Reid², K. M. Menten¹, X. W. Zheng³, L. Moscadelli⁴, and Y. Xu^{1,5}

ABSTRACT

We report trigonometric parallaxes for the massive star-forming regions G23.01–0.41 and G23.44–0.18, corresponding to distances of $4.59^{+0.38}_{-0.33}$ kpc and $5.88^{+1.37}_{-0.93}$ kpc, respectively. The distance to G23.01–0.41 is smaller than its near kinematic distance assuming a standard model of the Milky Way and less than half of its far kinematic distance, which has usually been assumed. This places it in the Crux-Scutum spiral arm. The distance to G23.44–0.18 is close to its near kinematic distance and most likely places it in the Norma spiral arm near the end of the Galactic bar. Combining the distance and proper motions with observed radial velocities gives the location and full space motion of the star forming regions. We find large deviations from circular Galactic orbits for these sources: both sources show peculiar motions of 20 to 30 km s^{−1} counter to Galactic rotation and toward the Galactic center. These large peculiar motions might be the result of gravitational perturbations from the Galactic bar.

Subject headings: techniques: interferometric – astrometry – Galaxy: structure – Galaxy: kinematics and dynamics – individual (G23.01–0.41, G23.44–0.18)

1. Introduction

As part of a large program to determine Galactic structure by measuring trigonometric parallaxes and proper motions of newly formed stars, we are conducting multi-epoch VLBA

¹Max-Planck-Institut für Radioastronomie, Auf dem Hügel 69, 53121 Bonn, Germany

²Harvard-Smithsonian Center for Astrophysics, 60 Garden Street, Cambridge, MA 02138, USA

³Department of Astronomy, Nanjing University, Nanjing 210093, China

⁴INAF, Osservatorio Astrofisico di Arcetri, Largo E. Fermi 5, 50125 Firenze, Italy

⁵Purple Mountain Observatory, Chinese Academy of Sciences, Nanjing 210008, China

observations of methanol masers associated with high-mass star forming regions. The motivation and background information regarding our program are discussed in Reid et al. (2008), hereafter called Paper I.

In this paper, we report observations of 12 GHz methanol masers toward two regions of high-mass star formation: G23.01–0.41 and G23.44–0.18. These sources are toward Galactic longitude 23° and both have large Local Standard of Rest (LSR) velocities, suggesting they are at great distances. Since high-mass star forming regions define spiral arms, accurate parallaxes for these sources should help locate the inner spiral arms of the Galaxy. Additionally, the Galaxy is thought to possess a central bar that terminates near the longitude of these star forming regions. Thus, by locating the masers and measuring their 3-dimensional space motions, we hope to learn about the effects of the bar potential.

2. Observations and Calibration

We used the NRAO ¹ Very Long Baseline Array (VLBA) to observe the 12 GHz methanol masers in the two star forming regions G23.01–0.41 and G23.44–0.18. Paper I describes the general observational strategy and data calibration procedures. In this section, we describe only those aspects of the observations that are specific to these two sources.

The observations conducted under program BR100F were scheduled on 2005 October 28, 2006 March 22 and September 29, and 2007 March 18. These dates were chosen to sample the peaks of the parallax signature in Right Ascension only, as the amplitude of the signature in Declination is considerably smaller. The total observing time for each epoch was 10 hours.

For background position references, we observed two sources from the VLBA Calibrator Survey, J1825-0737 (Fomalont et al. 2003) and J1832-1035 (Petrov et al. 2006), and one source from a targeted VLA calibrator search, J1833-0855 (Xu et al. 2006). We used the ICRF source J1800+3848 (Ma et al. 1998) as a fringe finder. For the phase-referencing observations, we used four adjacent frequency bands with 4 MHz bandwidth in both right and left circular polarization. The second band contained the maser signals and was centered at an LSR velocity of 75.0 km s^{-1} for G23.01–0.41 and 103.0 km s^{-1} for G23.44–0.18.

We performed a “manual phase-calibration” using the data from J1800+3848 to remove instrumental phase offsets among the four frequency bands. We used a spectral channel with

¹The National Radio Astronomy Observatory is a facility of the National Science Foundation operated under cooperative agreement by Associated Universities, Inc.

Table 1. Source Information

Source	R.A. (J2000) (h m s)	Dec. (J2000) (° ' ")	ϕ (°)	P.A. (°)	V_{LSR} (km s ⁻¹)	Restoring Beam (mas, mas, deg)
G 23.01	18 34 40.27700	-09 00 38.4010	0	...	81.5	2.7 × 0.8 @ -14
J1825-0737 ...	18 25 37.60955	-07 37 30.0128	2.6	-58		2.1 × 0.7 @ -13
J1832-1035 ...	18 32 20.83656	-10 35 11.2006	1.7	-20		2.1 × 0.7 @ -12
J1833-0855 ...	18 33 19.58200	-08 55 27.2100	0.3	-75		2.1 × 0.7 @ -14
G 23.44	18 34 39.18690	-08 31 25.4050	0	...	97.6	3.3 × 2.0 @ -1
J1825-0737 ...	18 25 37.60955	-07 37 30.0128	2.4	-68		2.6 × 1.2 @ -4
J1832-1035 ...	18 32 20.83656	-10 35 11.2006	2.1	-15		2.7 × 1.2 @ -2
J1833-0855 ...	18 33 19.58200	-08 55 27.2100	0.5	-39		2.7 × 1.2 @ -2

Note. — ϕ and P.A. are the separations and position angles (East of North) between maser and reference sources. The radial velocity of the masers and the size and shape of the interferometer restoring beam are listed for the first epochs data.

one bright and compact maser feature as the phase reference: for G23.01–0.41 we used the channel at V_{LSR} of 81.54 km s^{-1} and for G23.44–0.18 the channel at 97.62 km s^{-1} .

3. Results

After calibration, we imaged the maser emission and the continuum sources using the AIPS task IMAGR. While all three background sources were clearly detected, J1832-1035 and J1833-0855 were heavily resolved and could not be used for high precision astrometry. Fig. 1 shows for the first epoch the images of J1825-0737 using G23.01–0.41 (left) and G23.44–0.18 (right) as the phase-reference. The small deviations from a point-like image are most likely caused by errors in the phase calibration due to short term fluctuations in the troposphere. Since the reference maser in G23.44–0.18 is resolved on the longest baselines, the data from the telescope on Mauna Kea could not be used for this source. This explains the different beam sizes for the sources in Table 1 and Fig. 1.

We estimated the positions of the masers and the background source by fitting elliptical Gaussian brightness distributions to the images. The positions of the maser spots relative to the background source were then modeled by the parallax sinusoid (including the effects of the ellipticity of the Earth’s orbit) and a proper motion in each coordinate. Since systematic errors generally dominate over random noise, formal position errors are usually unrealistic small. This results in relatively high χ^2 per degree of freedom values of the parallax fit (typically values between 2 and 8). The magnitude of the systematic errors are *a priori* unknown and can only be estimated from the goodness of the fits. Hence, we assigned independent “error floors” to the Right Ascension and Declination positions and added them in quadrature to the formal position fitting errors. The error floors were then adjusted until residual χ^2 per degree of freedom values of unity were achieved for each coordinate.

3.1. G23.01–0.41

The maser emission toward G23.01–0.41 consists of one bright and one weak spot separated by $\sim 45 \text{ mas}$ (see Fig. 2), both of which could be used for precision astrometry. The methanol maser position agrees within $0.3''$ with the position of a recently detected H_2CO maser and the peak of the NH_3 (3,3) emission (Araya et al. 2008). Table 2 and Fig. 3 show the results of the parallax and proper motion fit for each maser spot. The fact that we obtain equally good fits for the strong and the weak maser spot shows that our accuracy is not limited by the signal to noise ratio but by systematic errors. A combined fit, where the

positions of the two maser spots are fitted with one parallax but different proper motions yields a parallax of 0.218 with a formal uncertainty of ± 0.012 mas. However, since there appear to be significant correlation among the different spots at each epoch (as evidenced by a tendency for data to deviate from the fit in the same direction), we take a conservative approach and adopt a parallax uncertainty of ± 0.017 (i.e., multiplying the formal uncertainty by $\sqrt{2}$). Hence, we obtain a distance of $4.59_{-0.33}^{+0.38}$ kpc for G23.01–0.41.

Our measured distance is smaller than the near kinematic distance of 5.0 kpc, assuming IAU values for the distance to the Galactic center of $R_0 = 8.5$ kpc and for the circular rotation speed of the LSR of $\Theta_0 = 220$ km s⁻¹. The measured distance is only $\sim 43\%$ of the far kinematic distance, which has been assumed in most previous studies of this region (Codella et al. 1997; Furuya et al. 2008; Araya et al. 2008). Thus, physical sizes and luminosities have been overestimated in these studies by factors of 2.4 and 5.5, respectively. The near kinematic distance can be brought into better agreement with the measured parallax, if one uses a Galactic rotation model with $\Theta_0/R_0 = 29.5$ km s⁻¹ kpc⁻¹ (Reid & Brunthaler 2004).

The measured distance places G23.01–0.41 at a Galactocentric radius of 4.64 kpc. The proper motions of both maser spots are consistent with each other, indicating that internal motions are small, as observed in many methanol maser sources (Moscadelli et al. 2002). The average proper motion is -1.72 ± 0.04 mas y⁻¹ toward the East and -4.12 ± 0.3 mas y⁻¹ toward the North, corresponding to -37 ± 3 km s⁻¹ and -90 ± 10 km s⁻¹, respectively.

3.2. G23.44–0.18

Toward G23.44–0.18 we detected several maser spots within a region of sky of ~ 50 mas (see Fig. 4). Four maser spots could be used for astrometric measurements. Table 3 and Fig. 5 show the results of fitting for parallax and proper motion. The combined fit yields a parallax of 0.170 mas, with a formal uncertainty of ± 0.016 mas. As for G23.01–0.41, the post-fit (East) position residuals appear correlated, and we adopt the most conservative approach of assuming 100% correlation and multiplying the formal uncertainty by $\sqrt{4}$. Hence, we obtain a distance of $5.88_{-0.93}^{+1.37}$ kpc for G23.44–0.18. This translates to a Galactocentric radius of 3.9 kpc.

Our trigonometric parallax distance is in good agreement with the near kinematic distance of 5.6 kpc, but not the far distance of 10.0 kpc, assuming IAU values of $R_0 = 8.5$ and $\Theta_0 = 220$ km s⁻¹. Using $R_0=8.0$ kpc and $\Theta_0=236$ km s⁻¹ would yield a smaller kinematic distance of 5.1 kpc. The proper motions of the four maser spots are similar, and the average

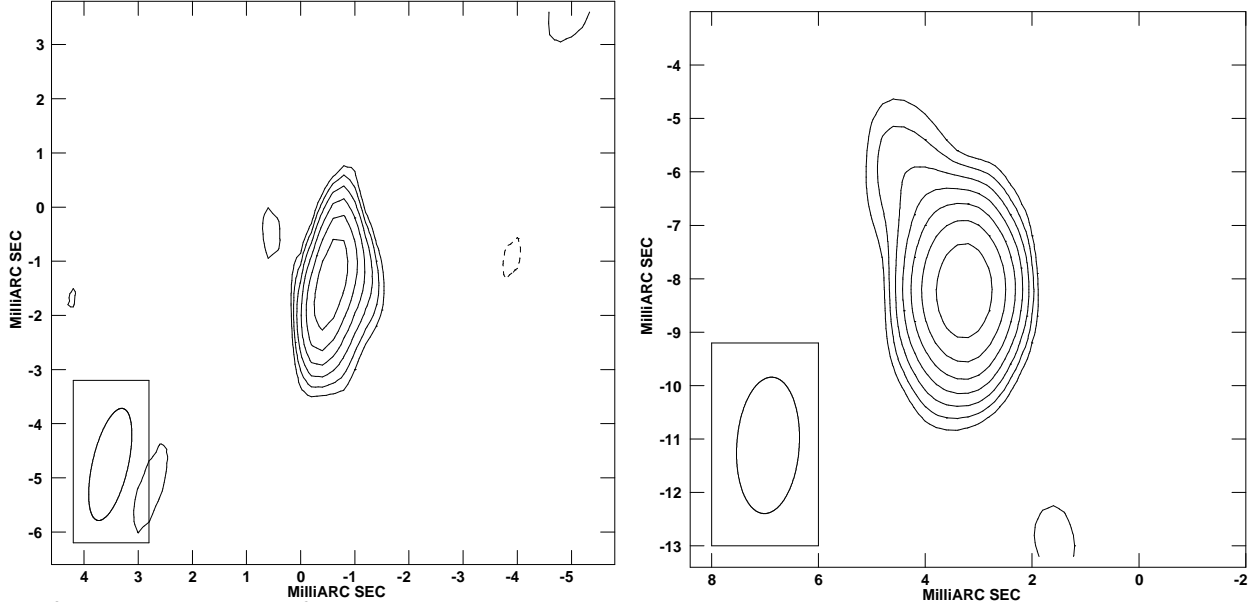


Fig. 1.— Phased-referenced images of J1825-0737 using G23.01–0.41 (left) and G23.44–0.18 (right) as reference source from the first epoch. The contours start at 12 mJy and increase with $\sqrt{2}$. Beam FWHM is indicated at lower left.

Table 2. G23.01-0.41 Parallax & Proper Motion Fits

Maser V_{LSR} (km s^{-1})	Background Source	Parallax (mas)	μ_x (mas y^{-1})	μ_y (mas y^{-1})
81.5	J1825-0737	0.217 ± 0.019	-1.74 ± 0.04	-4.11 ± 0.3
80.8	J1825-0737	0.221 ± 0.020	-1.70 ± 0.04	-4.13 ± 0.3
combined		0.218 ± 0.017		

Note. — Combined fit used a single parallax parameter for both maser spots relative to the background source; a single proper motion was fit for each maser spot relative to the background source.

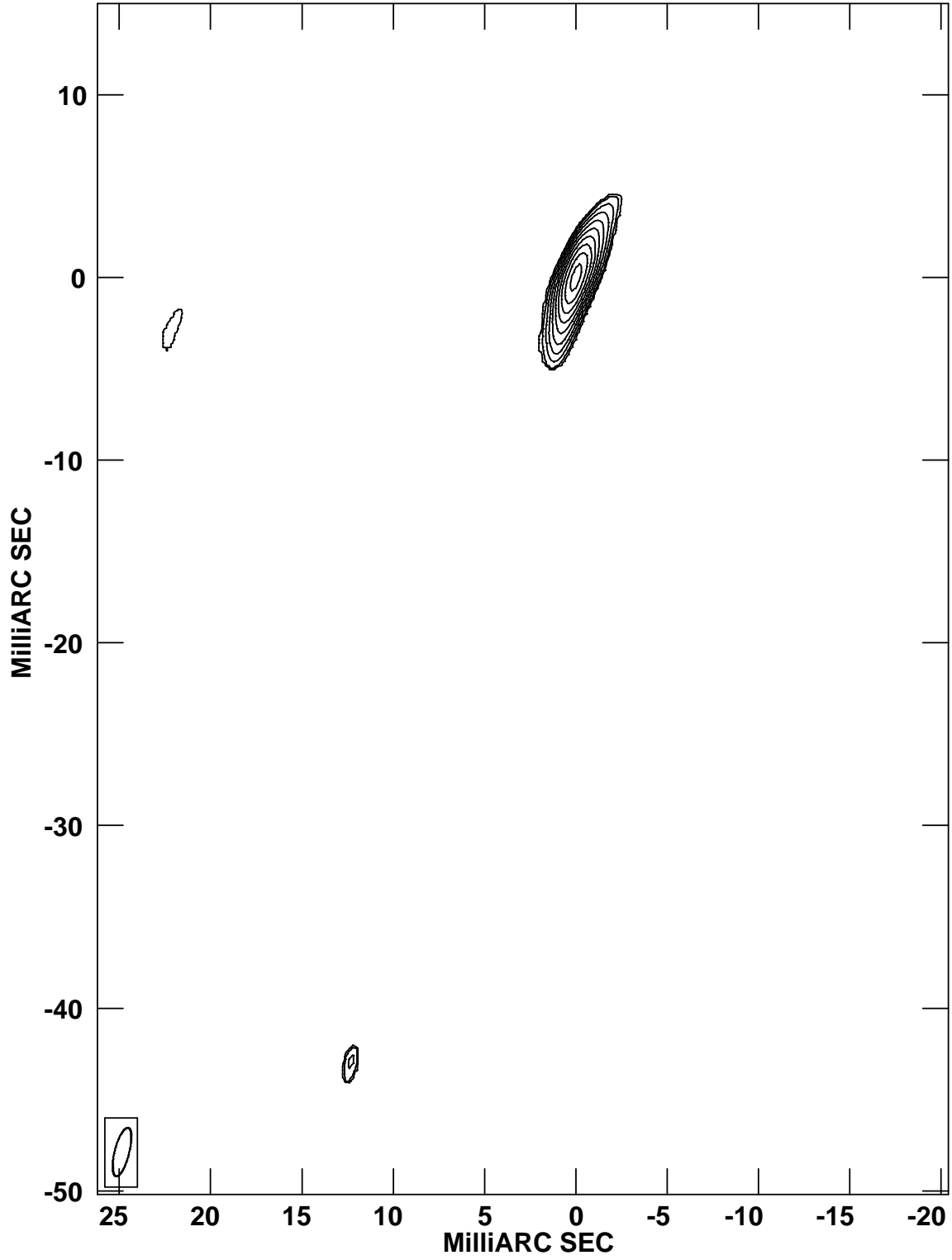


Fig. 2.— Velocity integrated maser emission of G23.01–0.41 in the first epoch. The contours start at 0.1 Jy km s^{-1} and increase with $\sqrt{2}$. Beam FWHM is indicated at lower left.

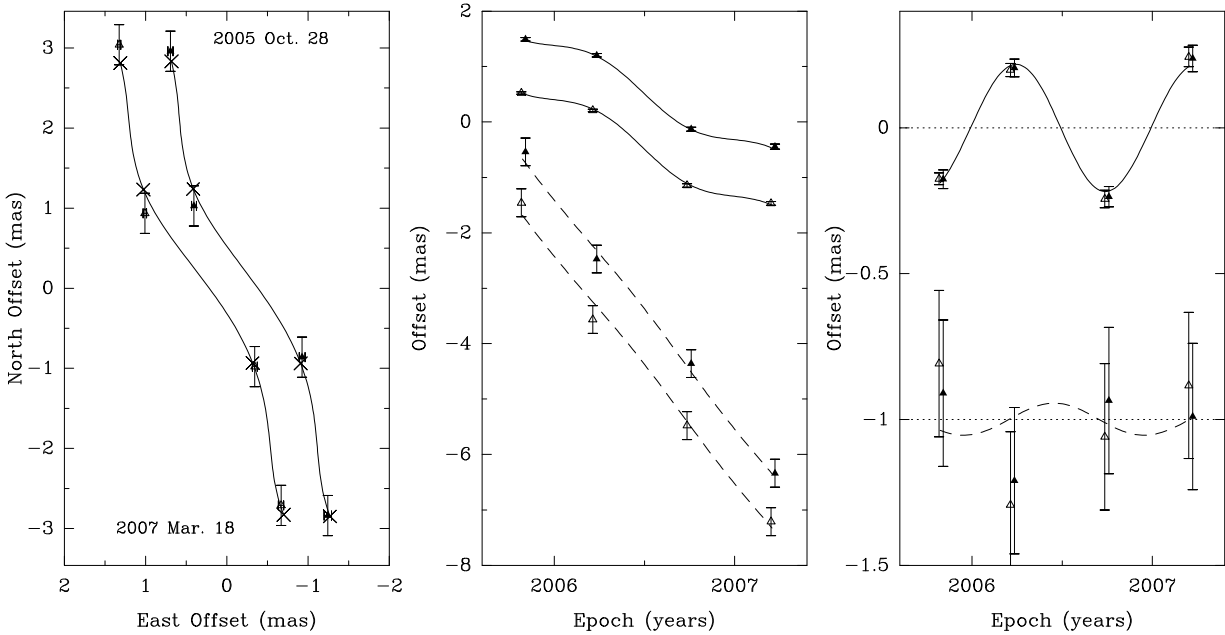


Fig. 3.— Results of the parallax fit for G23.01–0.41. The different symbols represent the two maser spots. **Left Panel:** Sky projected motion of the maser. The crosses and the lines show the best-fit position offsets and the trajectory, respectively. **Middle Panel:** The position offsets of the masers along the East and North direction versus time. The best-fit model in East and North direction are shown as continuous and dashed lines, respectively. **Right Panel:** Same as the middle panel but with fitted proper motions removed. The North offset data have been shifted for clarity.

motion is -1.93 ± 0.1 mas y^{-1} and -4.11 ± 0.07 mas y^{-1} , corresponding to -54 ± 10 km s^{-1} and 115 ± 22 km s^{-1} eastward and northward, respectively.

4. Discussion

Our measurements not only locate two sources in the Galaxy, they also provide the full space motion of each star-forming region. A useful reference frame for Galactic dynamics removes a model of Galactic rotation and yields peculiar motion relative to each source’s “local standard of rest.” We define Cartesian motion components U_s, V_s, W_s locally toward the Galactic center, toward direction of rotation, and toward the North Galactic Pole. The methods used to convert the measured (heliocentric) proper motions into this frame will be described in detail in an upcoming paper.

If one adopts the IAU values for the LSR motion ($R_0 = 8.5$ and $\Theta_0 = 220$ km s^{-1}) and the Hipparcos values for the Solar Motion (Dehnen & Binney 1998), we obtain the peculiar motion components listed in Table 4. Both masers move significantly slower (~ 25 km s^{-1}) than Galactic rotation and have large peculiar motions (~ 30 km s^{-1}) toward the Galactic center. The peculiar motions toward the Galactic center could be reduced were one to use a rotation model of the Milky Way that is consistent with the measured proper motion of Sgr A*, the super-massive black hole at the Galactic center (Reid & Brunthaler 2004). However, changing the rotation model does not significantly reduce the peculiar motions in the direction of Galactic rotation (Table 5).

Benjamin et al. (2005) find a stellar overdensity in the inner Galaxy, which can be explained with a central bar with half-length $R_{\text{bar}} = 4.4 \pm 0.5$ kpc, tilted by $\Phi = 44^\circ \pm 10^\circ$ to the Sun-Galactic center line. Other studies find smaller angles of $24^\circ - 27^\circ$ between the major axis of the bar and the Sun-Galactic center and prefer a shorter bar (Gerhard 2002; Rattenbury et al. 2007). Possibly there are multiple components to the bar.

Our two star forming regions, in particular G23.44–0.18 are located close to the end of the central bar (Fig. 6). This raises the question, whether the large peculiar motions of the sources are induced by the gravitational potential of the central bar. Roberts et al. (1979) show that a barlike potential can induce strong noncircular motions in the gas flow of $\sim 50 - 150$ km s^{-1} . Shocks may move gas in the inner parts outward and gas in the outer parts inward in a region, thus focusing gas where the spiral arm bends from the bar. The space motions of our maser sources inward toward the Galactic center are qualitatively consistent with such bar shocks.

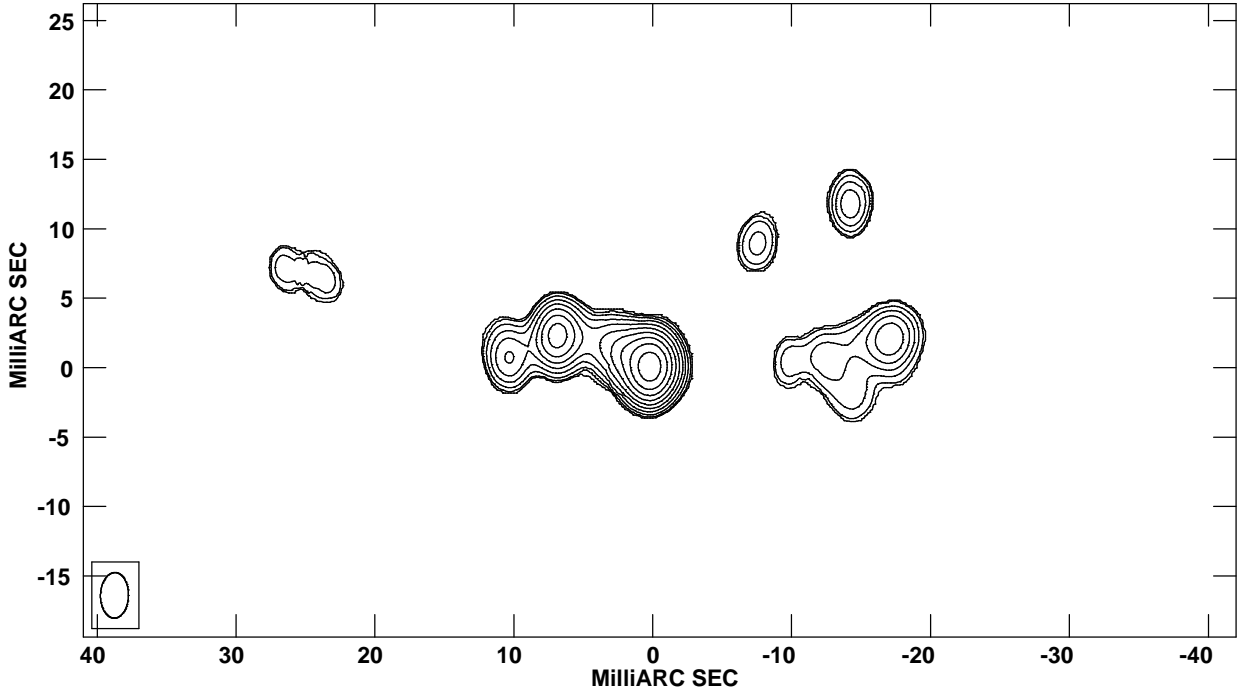


Fig. 4.— Velocity integrated maser emission of G23.44–0.18 in the first epoch. The contours start at 0.1 Jy km s^{-1} and increase with $\sqrt{2}$. Beam FWHM is indicated at lower left.

Table 3. G23.44-0.18 Parallax & Proper Motion Fits

Maser V_{LSR} (km s^{-1})	Background Source	Parallax (mas)	μ_x (mas y^{-1})	μ_y (mas y^{-1})
98.4	J1825-0737	0.179 ± 0.055	-1.97 ± 0.10	-4.05 ± 0.09
97.2	J1825-0737	0.159 ± 0.028	-1.87 ± 0.05	-4.08 ± 0.04
96.9	J1825-0737	0.138 ± 0.057	-1.88 ± 0.10	-4.12 ± 0.09
96.5	J1825-0737	0.230 ± 0.046	-1.99 ± 0.08	-4.18 ± 0.09
combined		0.170 ± 0.032		

Note. — Combined fit used a single parallax parameter for the four maser spots relative to the background source; a single proper motion was fit for each maser spot relative to the background source.

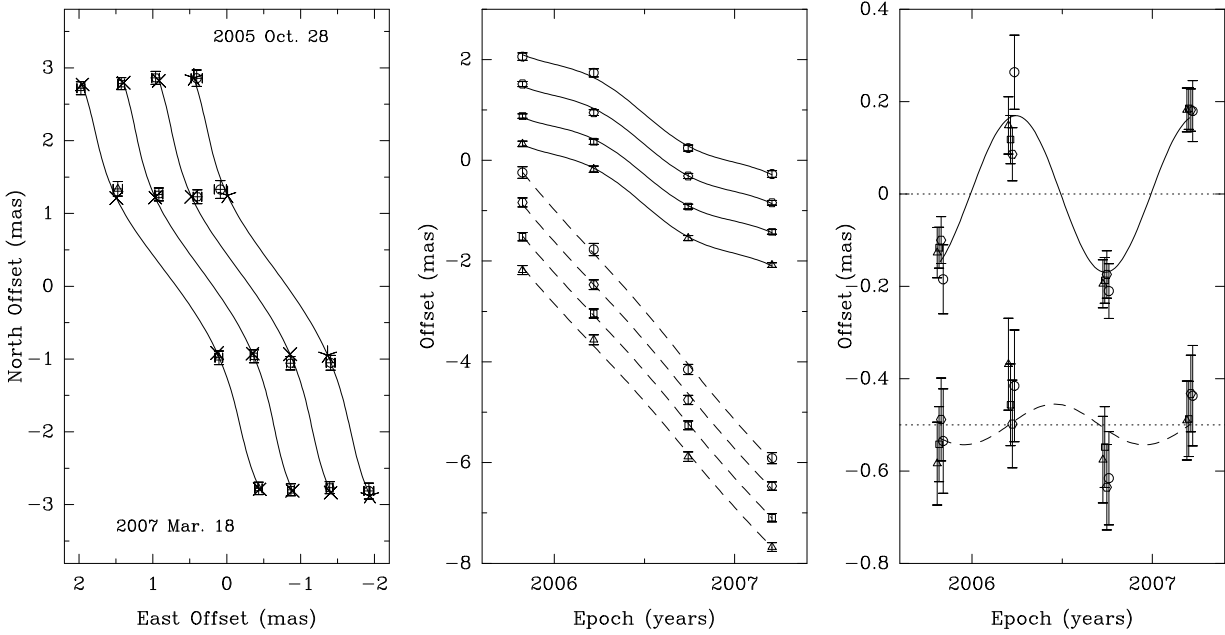


Fig. 5.— Results of the parallax fit for G23.44–0.18. The different symbols represent the four maser spots. **Left Panel:** Sky projected motion of the maser. The crosses and the lines show the best-fit position offsets and the trajectory, respectively. **Middle Panel:** The position offsets of the masers along the East and North direction versus time. The best-fit model in East and North direction are shown as continuous and dashed lines, respectively. **Right Panel:** Same as the middle panel but with fitted proper motions removed. The North offset data have been shifted for clarity.

Table 4. Peculiar Motions

Maser	U_s (km s^{-1})	V_s (km s^{-1})	W_s (km s^{-1})
G23.01–0.41	37 ± 6	-29 ± 12	-1.4 ± 3
G23.44–0.18	23 ± 12	-26 ± 15	1.9 ± 3

Note. — Peculiar motions assuming $R_0=8.5$, $\Theta_0=220 \text{ km s}^{-1}$, and the Hipparcos Solar Motion (Dehnen & Binney 1998). U_s is toward the Galactic center, V_s is toward Galactic rotation, and W_s is toward the North Galactic Pole.

Table 5. Same as Table 4 but for $R_0=8.0$ and $\Theta_0=236 \text{ km s}^{-1}$

Maser	U_s (km s^{-1})	V_s (km s^{-1})	W_s (km s^{-1})
G23.01–0.41	21 ± 5	-29 ± 8	-1.4 ± 3
G23.44–0.18	-5 ± 11	-26 ± 13	1.9 ± 3

Andreas Brunthaler was supported by the DFG Priority Programme 1177. Ye Xu was supported by Chinese NSF through grants NSF 10673024, NSF 10733030, NSF 10703010 and NSF 10621303.

REFERENCES

- Araya E. D., Hofner P., Goss W. M., et al., 2008, ArXiv e-prints, 0806.1548
- Bartkiewicz A., Brunthaler A., Szymczak M., van Langevelde H. J., Reid M. J., 2008, *A&A*, 490, 787
- Benjamin R. A., Churchwell E., Babler B. L., et al., 2005, *ApJ*, 630, L149
- Codella C., Testi L., Cesaroni R., 1997, *A&A*, 325, 282
- Dehnen W., Binney J. J., 1998, *MNRAS*, 298, 387
- Fomalont E. B., Petrov L., MacMillan D. S., Gordon D., Ma C., 2003, *AJ*, 126, 2562
- Furuya R. S., Cesaroni R., Takahashi S., et al., 2008, *ApJ*, 673, 363
- Gerhard O., 2002, The Galactic Bar, in *Astronomical Society of the Pacific Conference Series*, Vol. 273, Da Costa G. S., Jerjen H. (eds.), *The Dynamics, Structure & History of Galaxies: A Workshop in Honour of Professor Ken Freeman*, p. 73
- Ma C., Arias E. F., Eubanks T. M., et al., 1998, *AJ*, 116, 516
- Moscadelli L., Menten K. M., Walmsley C. M., Reid M. J., 2002, *ApJ*, 564, 813
- Petrov L., Kovalev Y. Y., Fomalont E. B., Gordon D., 2006, *AJ*, 131, 1872
- Rattenbury N. J., Mao S., Sumi T., Smith M. C., 2007, *MNRAS*, 378, 1064
- Reid M. J., Brunthaler A., 2004, *ApJ*, 616, 872
- Reid M. J., Menten M. K., Brunthaler A., et al., 2008, *ApJ*, submitted, arXiv:0811.0595
- Roberts W. W., Jr., Huntley J. M., van Albada G. D., 1979, *ApJ*, 233, 67
- Xu Y., Reid M. J., Menten K. M., Zheng X. W., 2006, *ApJS*, 166, 526

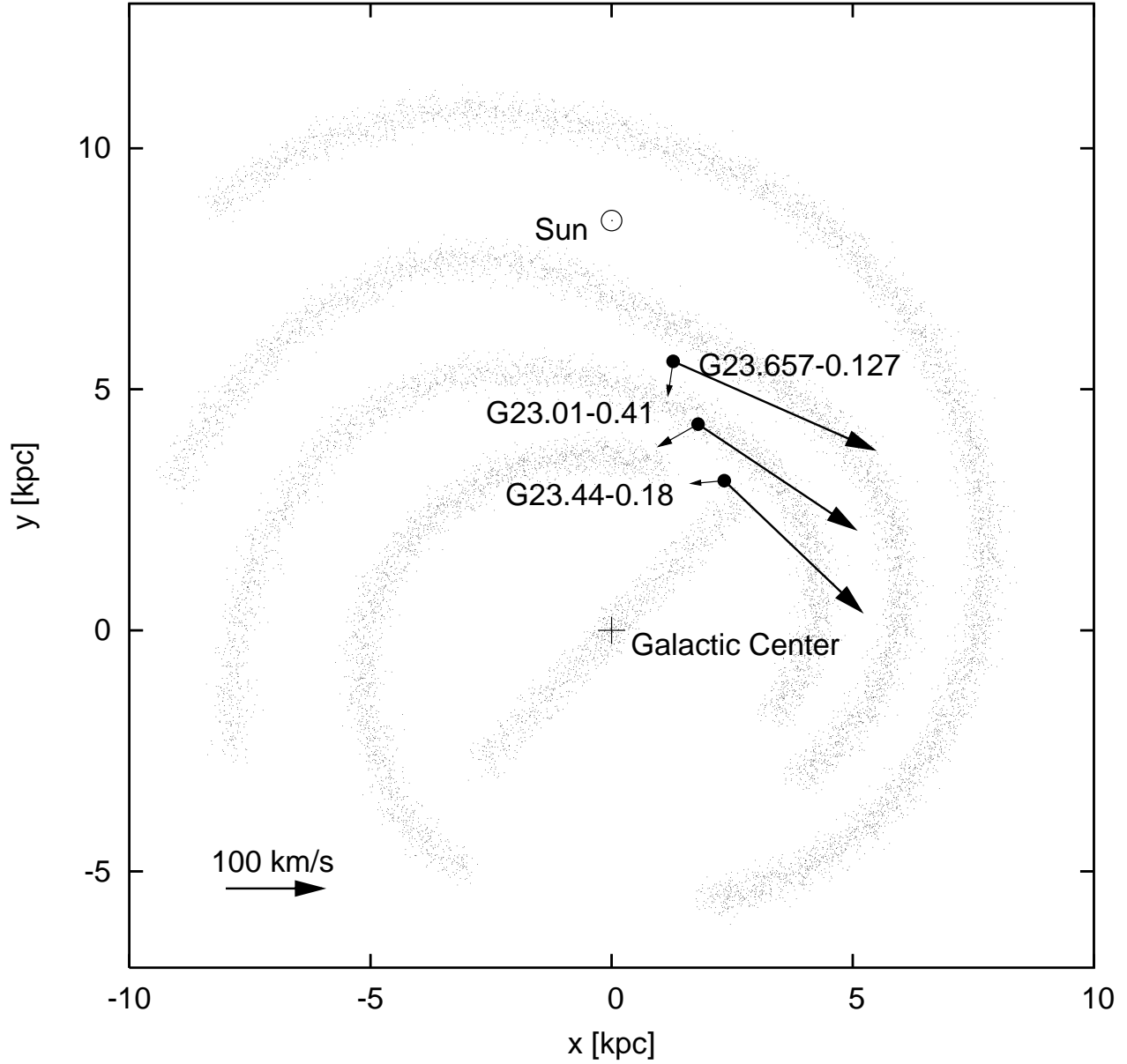


Fig. 6.— Schematic view of the Milky Way with the positions of G23.01–0.41 and G23.44–0.18, their total motion relative to the Galactic Center (long arrows), and their peculiar motion after removing Galactic rotation (short arrows). The IAU values of $R_0=8.5$ kpc and $\Theta_0=220$ km s $^{-1}$ are assumed. Also shown is the location of the central bar from Benjamin et al. (2005) and the position and motion of G23.657-0.127 by Bartkiewicz et al. (2008).